ACS APPLIED MATERIALS & INTERFACES

Research Article

www.acsami.org

Direct Carbonization of Cyanopyridinium Crystalline Dicationic Salts into Nitrogen-Enriched Ultra-Microporous Carbons toward Excellent CO_2 Adsorption

Guojian Chen, Xiaochen Wang, Jing Li, Wei Hou, Yu Zhou,* and Jun Wang*

State Key Laboratory of Materials-Oriented Chemical Engineering, College of Chemistry and Chemical Engineering, Nanjing Tech University, Nanjing 210009, P. R. China

Supporting Information

ABSTRACT: A family of nitrogen-enriched ultramicroporous carbon materials was prepared by direct carbonization of task-specifically designed molecular carbon precursors of cyanopyridinium-based crystalline dicationic salts (CISs). Varying the molecular structure of CISs, large surface area (918 $m^2\ g^{-1}$), high N content (20.10 wt %), and narrow distributed ultramicropores (0.59 nm) can be simultaneously achieved on the sample PCN-14 derived from methyl-linked 4-cyanopyridinium D[4-CNPyMe]Tf_2N. It therefore exhibited exceptional performance in greenhouse gas CO_2 capture, i.e., simultaneously possessing (1) high CO_2 adsorption uptakes: 5.33 mmol g^{-1} at 273 K, and 3.68 mmol g^{-1} at 298 K (both at 1.0 bar); (2) unprecedented selectivity of CO_2 versus N_2: 156; and (3) a high adsorption ratio of CO_2 to N_2: 148 (at 1.0 bar). This is the first time such a high selectivity and adsorption ratio over carbon materials has been achieved, which is among the highest values over solid adsorbents.

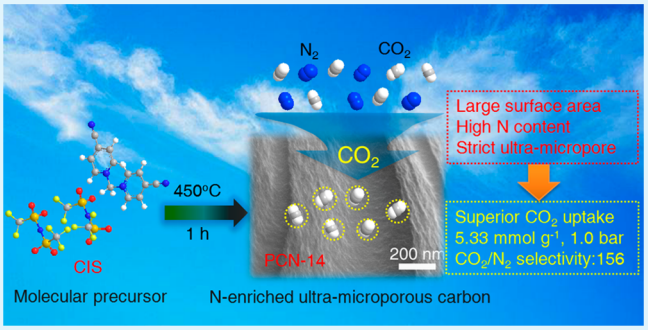

KEYWORDS: *CO_2 capture, microporous materials, porous carbon, ionic liquids, molecular precursors*

INTRODUCTION

Nanoporous carbon materials attract increasing attention and exhibit diverse applications in energy,[1] the environment,[2] catalysis,[3] adsorption, and separation,[4] because of the large surface area, high chemical and physical stability, tailored pore architectures, and surface properties.[5] Various porous carbons with multiscale pore structures have been specifically designed, including microporous, ordered/disordered mesoporous, macroporous, and hierarchical porous carbons.[6,7] It has been an increasingly hot topic to task-specifically and facilely design new carbon materials with high performances. Among various strategies to achieve carbon materials,[8−14] direct carbonization is demonstrated to be very efficient due to the avoidance of any templates or post-treatments, motivating the development of various promising carbon precursors, such as microporous organic polymers (MOPs),[15−17] metal−organic frameworks (MOFs),[18,19] biomass and derivatives,[20] and ionic liquids (ILs).[21] However, it is still a very difficult issue to precisely control the synthesis of the desirable porous carbon materials for specific applications.

The sharply rising level of CO_2 in the atmosphere has urged the development of effective CO_2 capture and sequestration technologies to reduce the emissions of greenhouse gases.[22] Current CO_2 adsorption and separation are dominated by amine-based absorption regeneration processes, limited by energy-cost, corrosion, and inefficiency.[23] As a result, a wide variety of alternative porous solid adsorbents have been prepared and used in CO_2 capture for high adsorption capacity and good regeneration stability.[24−29] Among them, porous carbons are believed to be one of the most promising candidates for CO_2 capture due to their various advantageous internal properties, as mentioned before.[5,29] Most commercial activated carbons exhibit moderate CO_2 uptakes due to the weak physisorption in undecorated carbon frameworks.[30] Therefore, much effort has been proposed to prepare porous carbon materials with high CO_2 adsorption capacity.[13−20] However, these carbons still suffered from inferior selectivity (e.g., CO_2/N_2 selectivity ranging from 18 to 79)[17,18,29,31] compared to those of microporous organic polymers (MOPs, CO_2/N_2 selectivity >100),[32,33] in spite of the higher CO_2 adsorption capacity over the former rather than the latter. Besides, the CO_2/N_2 selectivity over carbons dropped rapidly with the increase of pressure (e.g., up to 1.0 bar), giving a much lower adsorption ratio of CO_2 to N_2. The reason can be assigned to the essential physical adsorption property that cannot provide enough CO_2-affinity and N_2-phobic at high pressure. The above-described phenomena can also be observed over those MOPs with high CO_2/N_2 selectivities.

Received: June 2, 2015
Accepted: July 30, 2015
Published: August 1, 2015

DOI: 10.1021/acsami.5b04842
ACS Appl. Mater. Interfaces 2015, 7, 18508−18518

Scheme 1. Preparation of the Typical N-Enriched Ultra-Microporous Carbon PCN-14 Directly Carbonized from the Newly Designed Cyanopyridinium Crystalline Dicationic Salt (CIS) Precursor D[4-CNPyMe]Tf_2N

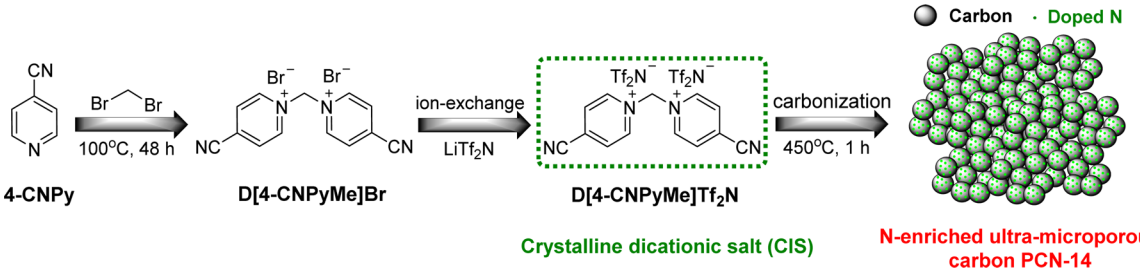

Presently, it remains a huge challenge to simultaneously achieve excellent CO_2/N_2 selectivity with high CO_2 adsorption capacity.

Previous works have pointed out that CO_2 capture over carbon is closely related to its porosity and surface chemical state. Current strategies toward high-performance carbons focus on the modification of surface compositions (e.g., the doping of heteroatoms) and pore structure control.[34−43] Incorporating heteroatoms such as nitrogen (N) into the carbon matrix has been demonstrated as a remarkable strategy to enhance CO_2 capture by virtue of the improved affinity interaction between acidic CO_2 molecules and N active basic sites.[34−39] Besides, it has also been indicated that the rich and narrowly distributed micropores smaller than 1.0 nm favor both CO_2 adsorption capacity and selectivity.[40−43] However, no such carbon material containing both high N content and strictly ultramicroporous structure has appeared, which may account for the current inferior selective capture capacity of CO_2.

In this work, we develop a new family of molecular level carbon precursors, i.e., cyanopyridinium crystalline dicationic salts (named as CISs), which are directly carbonized to fabricate N-enriched ultramicroporous carbon series (PCNs) at a relatively low temperature of 450 °C without any additives or pre/post-treatments (Scheme 1). As is known, molecular carbon precursors benefit from finely controlling the composition and pore structure of the target carbon materials, but rarely can they be directly carbonized to porous carbons.[44] Some special ILs with cross-linkable groups (e.g., cyano group) or protic ionic liquids/salts were promising carbon precursors for directly producing micro/mesoporous carbons with large surface areas and high N contents.[45−49] Those IL-derived carbons showed moderate CO_2 uptakes of 2.0−3.0 mmol g^{-1} (298 K and 1.0 bar) and low CO_2/N_2 selectivities of 20−37.[47,49] Herein, the molecular precursors of CISs are task-specifically designed by quaternization reaction of 4-/3-cyanopyridine with dibromomethane with successive anion-exchange of the commercially available bulky anion [Tf_2N] (bis(trifluoromethanesulfonyl)imide). These CISs have similar structures to common ILs but own well-defined crystalline structures and high melting points (most of them >140 °C). Detailed systemic study is performed over the carbonization process, revealing that the porosities and N contents of the obtained CISs-derived PCNs can be tailored by elaborately adjusting alkyl and alkylaryl (i.e., methyl, ethyl, butyl, xylyl, and dixylyl) halide organic linkers and the positions of cyano groups on pyridine rings. The intrinsic cyano groups fasten to pyridine rings, and the bulky anions play key roles in the formation of the strict ultramicropores (<0.7 nm). Large surface area (918 m^2 g^{-1}), high N content (20.1 wt %), and narrow ultra-micropores (0.59 nm) are simultaneously achieved on the typical carbon sample of PCN-14, enabling excellent CO_2 capture performances: (i) very high CO_2 uptakes (5.33 mmol g^{-1} at 273 K, 1.0 bar and 3.68 mmol g^{-1} at 298 K, 1.0 bar); (ii) unprecedented CO_2/N_2 selectivity (156 at 273 K); and (iii) the high adsorption ratio of CO_2 to N_2 (148 at 273 K, 1.0 bar). This work breaks through the inferior CO_2/N_2 selectivity over previous porous carbons, while also giving a high CO_2 adsorption capacity.

EXPERIMENTAL SECTION

Materials. 4-Cyanopyridine, 3-cyanopyridine, pyridine, dibromomethane, 1,2-dibromoethane, 1,4-dibromobutane, α,α'-dichloro-*p*-xylene, 4,4′-bis(chloromethyl)biphenyl, the required solvents and lithium bis(trifluoromethanesulfonyl)imide ($LiTf_2N$) were purchased from Aladdin and Sinopharm Chemical and used without further purification.

Characterization. Liquid-state ^1H and ^{13}C NMR spectra were measured with a Bruker DPX 500 spectrometer at ambient temperature in the solvents of D^6-DMSO using TMS as internal reference. The solid state cross-polarization magic angle spinning (CP/MAS) ^{13}C NMR spectrum was recorded on a Bruker Avance III 400 NMR spectrometer. Melting points (mp) were measured using an X4 digital microscopic melting point apparatus with an upper limit of 250 °C. Fourier transform infrared spectroscopy (FT-IR) was recorded on a Nicolet iS10 FT-IR instrument (KBr discs) in the region 4000−400 cm^{-1}. X-ray photoelectron spectra (XPS) were conducted on a PHI 5000 Versa Probe X-ray photoelectron spectrometer equipped with Al Kα radiation (1486.6 eV). Raman spectra were recorded on a Jobin Yvon (Laboratory RAM HR1800) confocal micro-Raman spectrometer backscattered geometry through a 10x (NA = 0.25) microscope objective, and an Ar^+ laser emitting at a wavelength of 514.5 nm was used as a source of excitation. The CHNS elemental analysis was performed on an elemental analyzer Vario EL cube. Thermogravimetric analysis (TGA) was carried out with a STA409 instrument under N_2 atmosphere at a heating rate of 10 °C min^{-1}. X-ray diffraction (XRD) measurements were made with a SmartLab diffractometer (Rigaku Corporation) equipped with a 9 kW rotating-anode Cu source at 40 kV and 200 mA, from 5° to 80° with a scan rate of 0.2° s^{-1}. Field emission scanning electron microscopy (FESEM; Hitachi S-4800, accelerated voltage: 5 kV) accompanied by Energy dispersive X-ray spectrometry (EDS; accelerated voltage: 20 kV) were used to study the morphology and the element mapping distribution. Transmission Electron Microscopy (TEM) images were obtained using a JEOL JEM-2100F 200 kV field-emission transmission electron microscope. N_2 adsorption isotherms were measured at 77 K with the BELSORP-MINI analyzer. Before measurement, the porous carbon samples were degassed for 3 h at 150 °C in a high vacuum. The gas (CO_2 and N_2) adsorption experiments were measured with a Micrometrics ASAP 2020 automatizm isothermal adsorption instrument. Prior to the measurements, the samples were degassed at 150 °C for 12 h.

Synthesis of Cyanopyridinium-Based Crystalline Dicationic Salts. Cyanopyridinium-based crystalline dicationic salts (CISs) were

DOI: 10.1021/acsami.5b04842
ACS Appl. Mater. Interfaces 2015, 7, 18508−18518

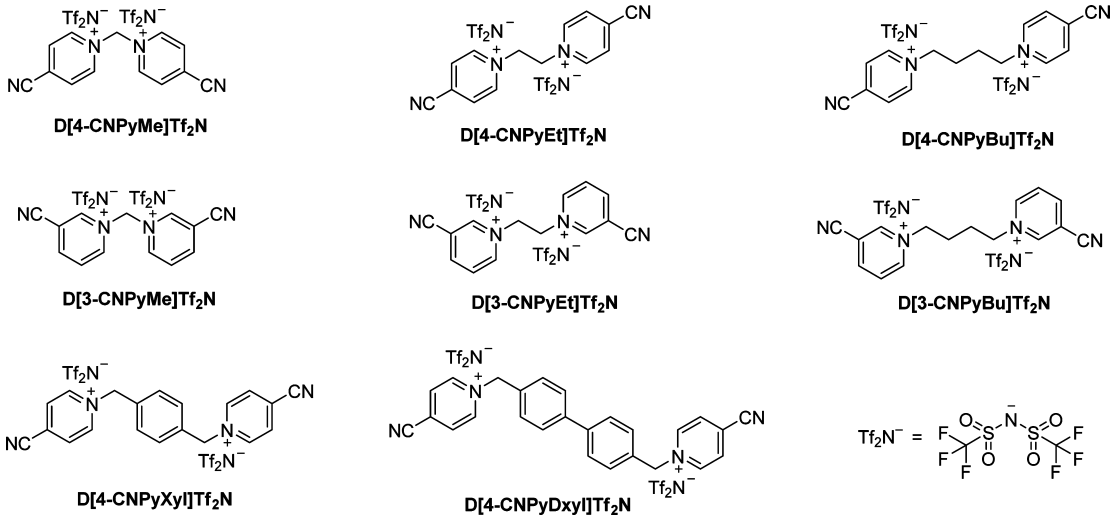

Figure 1. Molecular structures of all the CIS precursors prepared by linking 4-cyanopyridine or 3-cyanopyridine with various alkyl chains, methyl (Me), ethyl (Et), butyl (Bu), xylyl (Xyl), and dixylyl (Dxyl), and successive ion-exchange with $LiTf_2N$.

Table 1. Textural Properties and Elemental N Contents of CIS Precursors-Derived Porous Carbons and Their CO_2 Adsorption Performance

							CO_2 uptake (mmol g^{-1})[g]	
PCN-*xy* series[a]	CIS precursor	S_{BET}[b] (m^2 g^{-1})	V_{total}[c] (cm^3 g^{-1})	V_{micro}[d] (cm^3 g^{-1})	D_{HK}[e] (nm)	N[f] (wt %)	273 K	298 K
PCN-14	D[4-CNPyMe]Tf_2N	918	0.368	0.368	0.59	20.10	5.33	3.68
PCN-13	D[3-CNPyMe]Tf_2N	722	0.282	0.282	0.61	20.54	5.01	3.32
PCN-24	D[4-CNPyEt]Tf_2N	881	0.359	0.356	0.64	15.95	4.27	3.08
PCN-23	D[3-CNPyEt]Tf_2N	672	0.269	0.268	0.66	17.71	3.80	2.70
PCN-44	D[4-CNPyBu]Tf_2N	830	0.338	0.335	0.66	15.56	3.88	2.35
PCN-43	D[3-CNPyBu]Tf_2N	729	0.323	0.320	0.61	14.02	4.08	2.73
PCN-54	D[4-CNPyXyl]Tf_2N	838	0.956	0.691	0.66	8.35	3.59	2.36
PCN-64	D[4-CNPyDxyl]Tf_2N	1040	0.458	0.455	0.51	7.04	4.49	2.65

[a]PCN-*xy* were prepared at 450 °C. [b]Surface area calculated using the BET method. [c]Total pore volume calculated at P/P_0 = 0.99. [d]Micropore volume calculated using α_s-plot method. [e]Small micropore size calculated by the H−K method. [f]N content was measured by elemental analysis. [g]CO_2 uptakes were measured at 273 and 298 K, 1.0 bar.

prepared by one-step quaternization reaction of 4-cyanopyridine or 3-cyanopyridine with dibromoalkane without an additional solvent.

In a typical synthesis (Scheme 1), D[4-CNPyMe]Br, 1,1′-methyl-bis(4-cyanopyridinium) dibromide, was prepared by treating a homogeneous solution of 4-cyanopyridine (50 mmol, 5.21 g) and dibromomethane (8 mL) in a 25 mL Teflon-lined autoclave at 100 °C for 48 h. After reaction, the formed bulk yellow green solid was dispersed into ethyl acetate solution with vigorous stirring for 2 h. The yellow green product with a yield of 60% was obtained by filtration, washed with ethyl acetate several times, and dried. Successively, D[4-CNPyMe]Br (10 mmol, 3.82 g) was dissolved in 50 mL water, followed by addition of 50 mL aqueous solution of $LiTf_2N$ (20 mmol, 5.75 g) under vigorous stirring. A gray precipitate was immediately formed, and the mixture was further stirred for 48 h. The suspension was filtrated, washed with pure water several times, and dried at 100 °C to give the solid product D[4-CNPyMe]Tf_2N (1,1′-methyl-bis(4-cyanopyridinium)bis[bis(trifluoromethanesulfonyl)imide]), a grayish solid, yield of 72%, mp 145 °C. ^1H NMR (300 MHz, D^6-DMSO) (Figure S1A): δ 9.67−9.69 (4H), 8.84−8.91 (4H), and 7.39 (2H). ^{13}C NMR (75.5 MHz, D^6-DMSO) (Figure S1B): δ 147.60, 131.41, 129.73, 114.62, 77.68, and 39.50. Elemental analysis: Found: C, 26.10; H, 1.63; N, 10.84; S, 16.08. Calcd. for $C_{17}H_{10}N_6F_{12}S_4O_8$ (782.54): C, 26.09; H, 1.29; N, 10.74; S, 16.39%. Other CIS precursors were prepared similarly, and details are shown in the Supporting Information (SI).

Preparation of N-Enriched Porous Carbon Materials. In a typical synthesis, 0.5 g CIS precursor D[4-CNPyMe]Tf_2N was placed in a quartz boat covered with aluminized paper and carbonized in a tube furnace. The sample was heated at a temperature of 450 °C at a ramp rate of 10 °C min^{-1} under nitrogen atmosphere and maintained at the final temperature for 1 h. Afterward, the tube furnace was slowly cooled down to room temperature to directly produce a typical N-doped microporous carbon with solid yield of 16.0%. The carbon sample was named PCN-14, in which 1 stands for the methyl linker, and 4 represents the 4-position of the CN group on the pyridine ring. In a similar process, a series of porous carbon samples with different yields in parentheses, PCN-13 (15.0%), PCN-24 (25.2%), PCN-23 (20.4%), PCN-44 (22.1%), PCN-43 (25.3%), PCN-54 (18.2%), and PCN-64 (33.5%), are respectively carbonized from the corresponding precursor (see Figure 1) D[3-CNPyMe]Tf_2N, D[4-CNPyEt]Tf_2N, D[3-CNPyEt]Tf_2N, D[4-CNPyBu]Tf_2N, D[3-CNPyBu]Tf_2N, D[4-CNPyXyl]Tf_2N, and D[4-CNPyDxyl]Tf_2N.

RESULTS AND DISCUSSION

N-Enriched Ultramicroporous Carbons. Figure 1 shows the molecular structures of the task-specifically designed cyanopyridinium-based dicationic salts (shorten as CISs) prepared through the nucleophilic substitution between 4-/3-cyanopyridine and dibromoalkane organic linkers with successive ion-exchanging by $LiTf_2N$. All these CISs are crystalline ionic solids, as demonstrated by the XRD results (Figure S10), and most of them have high melting points exceeding 140 °C. TGA curves (Figure S11) indicate that they

DOI: 10.1021/acsami.5b04842
ACS Appl. Mater. Interfaces 2015, 7, 18508−18518

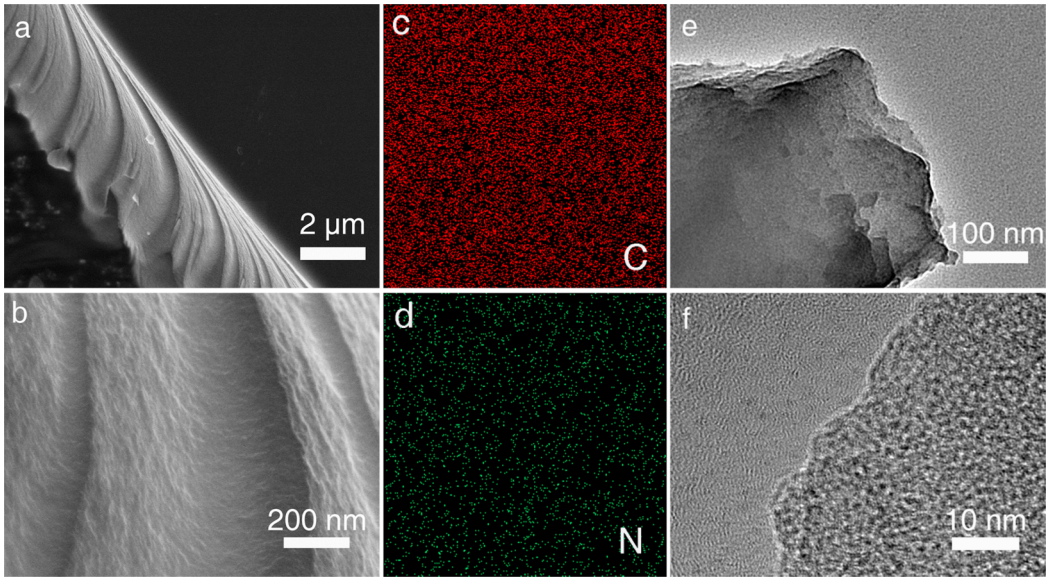

Figure 2. SEM images (a, b) of a typical N-enriched carbon PCN-14 and the corresponding EDS mapping images (the scale range referring to part b) for the elements of (c) carbon and (d) nitrogen, respectively, and TEM images (e, f) of PCN-14.

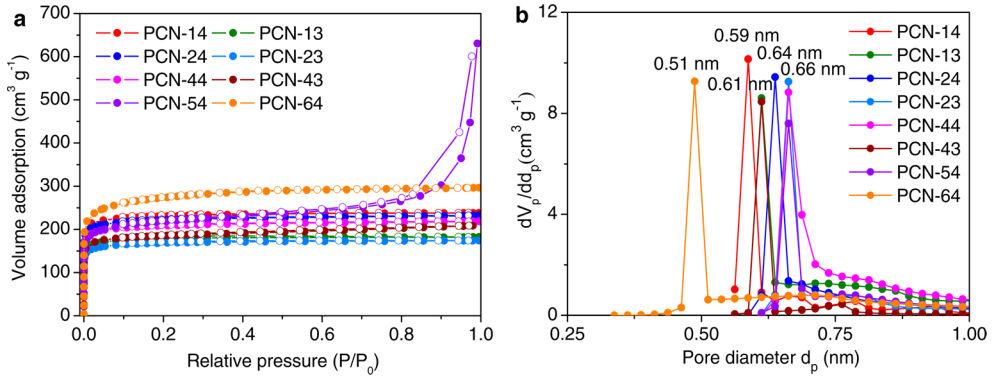

Figure 3. (a) N_2 adsorption−desorption isotherms of CIS-derived N-enriched porous carbons PCN-*xy*. (b) Micropore size distribution of PCN-*xy* series calculated by the H−K method.

possess good thermal stability with the initial decomposition temperatures higher than 250 °C, some of them even as high as 330 °C. These CISs can be directly carbonized into N-enriched ultramicroporous carbon materials without adding any catalyst, template, or chemical activator.

The carbon materials series PCN-*xy* (x = 1, 2, 4, 5, 6; y = 4, 3) derived from the corresponding CISs (Figure 1 and Table 1) are prepared by controlling the carbonization temperature at 450 °C (Table S1). By optimizing the carbonization duration, the desired carbon sample PCN-14 is obtained with a short hold time of 1 h (Figure S12 and Table S2). The XRD patterns are performed for all these samples (Figure S13 and S14), illustrating the loss of crystalline structures of CIS precursors and the formation of a carbon framework possessing a graphitic stacking peak (002) at 20.4−25.6° and an intralayer condensation peak (100) at the higher degree of 42.2−43.8°.[49,50] SEM images (Figure 2a and Figure S15) demonstrate that these obtained carbon materials are micron-sized carbon blocks with a compact surface. Highly magnified SEM images for the cross section indicate that one carbon block (>10 μm) is aggregated from very small intertwined nanoparticles sized at 10−20 nm without observing mesopores (Figure 2b and Figure S15), except for the sample PCN-54 prepared from xylyl-linked D[4-CNPyXyl]Tf_2N with nanoparticles (~30 nm) having a loosely aggregated morphology with distinct slit-like mesopores (Figure S15). Elemental analyses validate the contents of the doped N atom in these carbon materials (Table 1). The EDS elemental mapping analyses for C and N of the selected PCN-14 sample (Figure 2, parts c and d) reveal the homogeneous distribution of N on the surface. It is worth pointing out that the intrinsic N/C molar ratios in the CIS precursors determine the N contents of the correspondingly resultant carbon materials: the high N/C molar ratio in the precursor leads to a high N-content carbon product (Figure S16 and Table S3). As seen in Table 1, the N contents can be precisely tailored, ranging from 7.04 to 20.54 wt %. PCN-14 and PCN-13 possess the high N contents of 20.10 and 20.54 wt %, respectively, due to the highest N/C molar ratio (~0.355) in their CIS precursors.

Figure 3 depicts the N_2 sorption isotherms and pore size distribution curves of the PCN-*xy* series. The N_2 sorption isotherms of the samples obtained from carbonizing alkyl chain or dixylyl-linked CIS precursors (PCN-14, 13, 24, 23, 44, 43, and 64) are all type I (Figure 3a), indicative of typical microporous materials. The qualitative behavior of the isotherm represents a strictly microporous structure without mesoporos-

DOI: 10.1021/acsami.5b04842
ACS Appl. Mater. Interfaces 2015, 7, 18508−18518

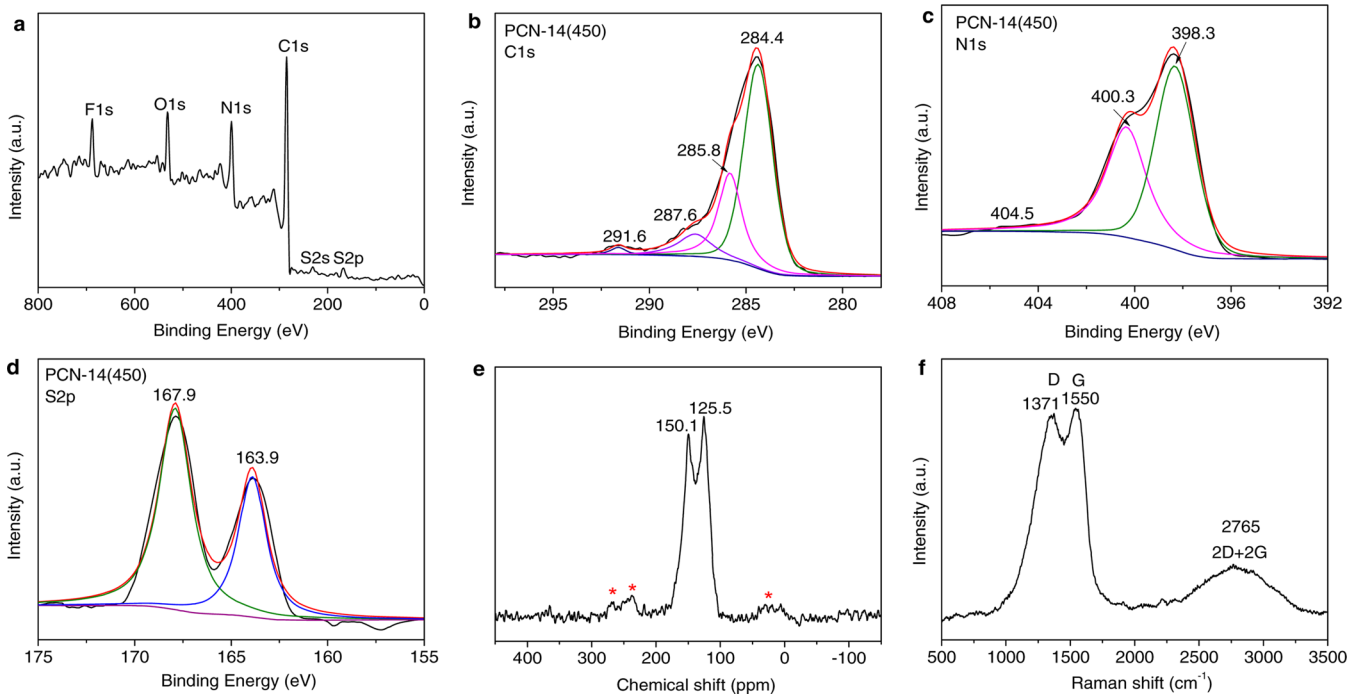

Figure 4. High resolution XPS spectra of N-enriched carbon PCN-14 prepared at 450 °C: (a) Survey, (b) C 1s, (c) N 1s, and (d) S 2p. (e) ^{13}C CP/MAS NMR spectrum. (f) Raman spectrum.

ity over these samples, in good accord with the compact morphologies observed in SEM images. One exception is the sample PCN-54 derived from xylyl-linked CIS precursor. Its N_2 sorption isotherm is type IV with an H1 hysteresis loop at P/P_0 = 0.80−0.99, indicating the presence of abundant mesopores originating from the nanovoids among the aggregated nanoparticles shown in the SEM image (Figure S15). The mesoporous aggregate architecture of PCN-54 can be associated with its specific molecular structure and distorted steric configuration with the rigid aromatic xylyl linker.[46,47] Figure 3b gives the micropore size distribution curves calculated by the Horvath−Kawazoe (H−K) method. All these PCN-*xy* samples demonstrate very narrow pore size distributions centered below 0.7 nm with a half peak width smaller than 0.03 nm. Such special porosity can be assigned to the ultramicroporous structure characteristic of small pore sizes lower than 0.7 nm, which is confirmed by the TEM images (Figure 2, parts e and f), which therefore implies the fabrication of N-enriched ultramicroporous carbon materials by direct carbonization of the molecular CISs.

The textural properties of the PCN-*xy* series (Table 1) reveal that they all possess high surface areas (672−1040 $m^2\ g^{-1}$) and large pore volumes. The exact porous structure, including the surface area, pore volume, and pore size of the obtained carbon materials, is also related to the molecular structures of CIS precursors (the length of carbon chains for organic linkers and the position of the CN group on pyridine rings). For alkyl chain linked CISs, shorter carbon chains yield higher surface areas for the final carbon materials; and the CN group at the 4 position of the pyridine ring also produces a higher surface area than the one at the 3 position of the pyridine ring. The situation is different using xylyl- or dixylyl-linked CISs. The sample PCN-54 with the rigid xylyl linker is a micro/mesoporous carbon material, while PCN-64 with the dixylyl linker possesses the highest surface area of 1040 $m^2\ g^{-1}$ and an ultrasmall micropore size of 0.51 nm. The steric configuration of CN groups on the pyridine rings can affect the polymerization of cyano groups and the carbonization process, and thus the more symmetric 4-CNPy-based CISs make for the formation of PCN products with higher surface areas.

The N contents and chemical states of the C, N, and S atoms for the selected sample PCN-14 are further evaluated by XPS, NMR, and Raman spectra. The XPS survey spectrum of PCN-14 (Figure 4a) presents five dominant peaks centered at 284.6, 398.3, 532.0, 688.0, and 167.9 eV, corresponding to the presence of C 1s, N 1s, O 1s, F 1s, and S 2p, respectively. The N content value of PCN-14 detected by XPS is 15.95 at% (16.84 wt %) on the surface, which is not far from the one (20.10 wt %) in the bulk carbon tested by elemental analysis, reflecting a relative homogeneous dispersion of the N atom, as demonstrated by the EDS elemental mapping analysis (Figure 2d). Figure 4, parts b and c, depicts the C 1s and N 1s core-level spectra, respectively. Fitting the C 1s spectrum with multiple peaks reveals a dominant peak at 284.4 eV corresponding to sp^2-hybridized graphitic carbon atoms and the other three peaks attributable to C═N (285.8 eV), pyridinic carbon C—N (287.6 eV), and C—S═O (291.6 eV), indicating that most of the carbon atoms are arranged in a conjugated honeycomb lattice.[49] The N 1s spectrum indicates that the N species mainly consist of pyridinic N (398.3 eV) and pyrrolic N (400.3 eV) originating from the pyridine and triazine rings, which are beneficial to CO_2 capture;[51] and a minor amount of oxidized N species is observed at higher binding energies (404.5 eV).[52] The S 2p spectrum shows the S species (3.25 wt %) doped in PCN-14, in agreement with the elemental analysis result (3.06 wt %, Table S1). The S 2p peak (Figure 3d) can be resolved into two peaks: the one located at 163.9 eV corresponds to neutral thiophene S and the other one located at 167.9 eV, attributable to oxidized S species from the $[Tf_2N]$ anion.[49] The solid-state ^{13}C CP/MAS NMR spectrum of PCN-14 gives two apparent signals for the formed N-doped graphitic carbon (Figure 4e). The peak at δ = 125.5 ppm is typical for all-

DOI: 10.1021/acsami.5b04842
ACS Appl. Mater. Interfaces 2015, 7, 18508−18518

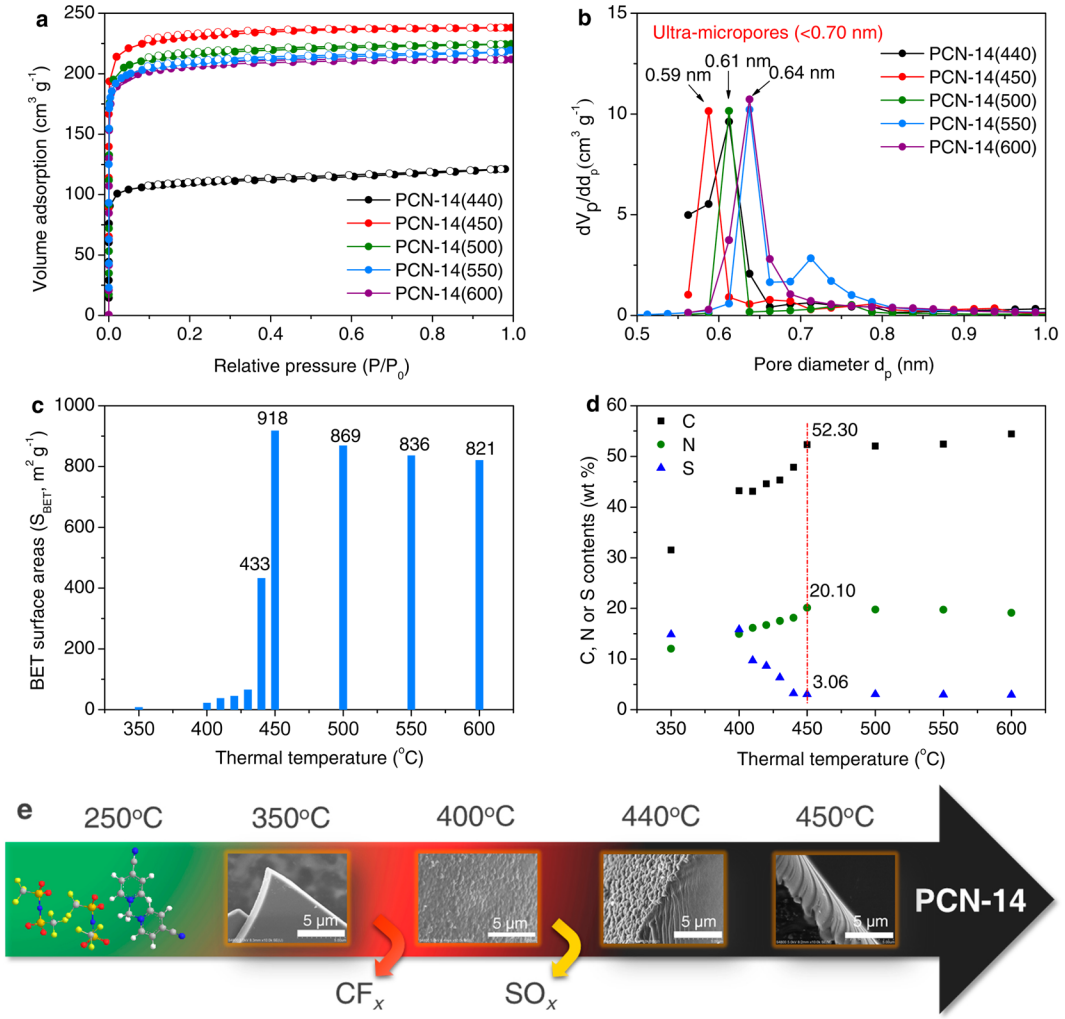

Figure 5. (a) N_2 sorption isotherms of N-enriched carbons PCN-14(T). (b) Micropore size distribution of PCN-14(T) series calculated by the H–K method. (c) BET surface areas (S_{BET}) values and (d) C, N, and S contents of PCN-14(T) as a function of the carbonization temperature. (e) Morphological variation and gas release process during the formation of PCN-14.

carbon-bonded aromatic carbons (C═C), while the peak at δ = 150.1 ppm is attributed to aromatic carbon bound to nitrogen atom (C═N).[50−52] The other weak board peaks (read asterisks) are assigned to the few residual CIS cations and [Tf_2N] anions.[51] The Raman spectrum of PCN-14 (Figure 4f) shows two intensive bands at 1550 (G band) and 1371 cm^{-1} (D band) featured for the ideal graphitic sp^2 carbons and disordered carbons, respectively.[53] Additionally, a broad intensity band at 2765 cm^{-1} (2D + 2G) is related to the defected carbons.

The above analyses demonstrate the formation of N-enriched ultramicroporous carbon materials with adjustable high surface area and pore structure determined by the molecular structure of CIS precursors. The results not only give rise to a promising porous solid adsorbent for selective CO_2 capture, but also provide a good opportunity to discuss the structure−activity relationship for subsequent applications.

Pore Formation Process. The formation process of carbon materials is studied by carbonizing D[4-CNPyMe]Tf_2N, the precursor for preparing PCN-14, at different temperatures. The TGA result (Figure S11) indicates that D[4-CNPyMe]Tf_2N begins to decompose at ca. 250 °C, losses 80% weight at 300 °C, and mainly completes the carbonization process at 450 °C. A series of N-enriched carbons named as PCN-14(T) are prepared with the carbonization temperature (T) from 350 to 600 °C and fully characterized by the N_2 sorption (Figure 5a), XRD (Figure S13), FT-IR (Figure S17), and SEM analyses (Figure S18 and Figure 5e). Table S1 lists the textural properties of these samples. With the low carbonization temperature of 350 °C, the obtained sample of PCN-14(350) is nonporous carbon (Table S1) with the morphology of micrometer scaled bulk blocks (Figure S18a). The XRD pattern shows that the crystalline structure of the precursor has disappeared at 350 °C, causing two weak broad peaks at about 21° and 33°, indicating its amorphous structure. As reported by previous work,[54] the cyano group in CIS should have undergone a trimerization reaction at 350 °C, which is represented by the appearance of a strong signal at 1351 cm^{-1} for the formation of triazine rings (FT-IR, Figure S17). The formed triazine-based polymeric cationic network is nonporous because the counterion [Tf_2N] still remains trapped within the polymeric network,[47,55] in agreement with the high S content of 14.84 wt % (Figure 5d and Table S1).

Heating the nonporous polymeric network at a higher temperature than 400 °C causes a dramatic morphological variation to interconnected submicron particles of 100−500 nm (Figure S18). The enhanced XRD signals are observed with slight variation of the peak position, but only a small surface

DOI: 10.1021/acsami.5b04842
ACS Appl. Mater. Interfaces 2015, 7, 18508−18518

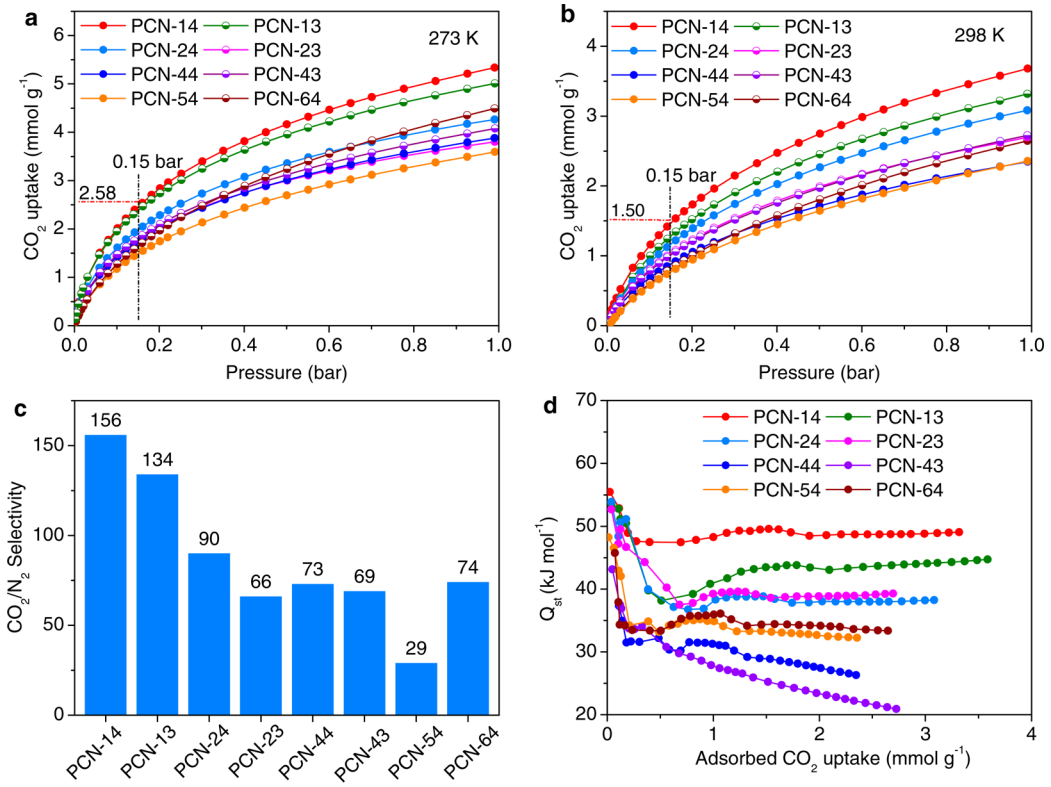

Figure 6. CO_2 sorption isotherms of PCN-*xy* samples at 273 K (a) and 298 K (b) under ambient pressure (1.0 bar). (c) CO_2/N_2 selectivities of PCN-*xy* series at 273 K, 1.0 bar. (d) Isosteric heats (Q_{st}) of CO_2 adsorption for PCN-*xy* series calculated using the Clausius−Clapeyron equation.

area is obtained (Figure 5c). The FT-IR adsorption bands (Figure S17) for CN groups (2254 cm^{-1}), pyridine rings (C—H, 3084 cm^{-1}; C═N, 1641 cm^{-1}), triazine rings (1351 cm^{-1}), CH_2 (2856, 2929, and 1466 cm^{-1}), and Tf_2N anion (C—F, S═O, 1180, 1134, 1049 cm^{-1}) become weakened or disappear, indicating the destruction of the polymeric network and decomposition of F- and S-containing bulky anion [Tf_2N]. The C, H, N, and S contents all increase (Figure 5d), suggesting that the release of the as-formed gases mainly related to CF_x (i.e., CF_4 and C_2F_6).[56] The above results indicate that the carbonization temperature up to 400 °C leads to the partial decomposition of the nonporous polymeric framework formed in a trimerization reaction, but the preservation of S species (15.84 wt %, Figure 5d), still forming the nonporous structure.

Increasing the carbonization temperature up to 430 °C causes a continuous decline of the S content and the slight increase of N content, while the C and H elements remain constant (Figure 5d), suggesting the release of a large amount of SO_x due to the decomposition of anions.[47,55] No obvious variation is observed from the SEM, FT-IR, and XRD. The slight shift of the XRD peaks to higher angles at 430 °C implies the gradual evolution to a graphitic phase. Superior surface area is achieved at 440 °C, accompanied by the further decline of S content (3.23 wt %) and the increase of C and N contents (Figure 5d). SEM images show that the morphology changes to be a compact block, the surface of which still exhibits the aggregation of interconnected particles but with a rough flat-like cross-section. An additional shift to higher angles at 25.6° for (002) peak and 43.0° for (100) peak is observed on the XRD pattern (Figure S13), revealing the formation of a graphitic phase carbon.[49] The N_2 sorption isotherm is type I, with a narrow pore size distribution centered at 0.61 nm (Figure 5, parts a and b). All of the above phenomena imply that the formation of N-enriched ultramicroporous carbon material begins at 440 °C, with a considerable surface area of 433 $m^2\ g^{-1}$ and a pore volume of 0.188 $cm^3\ g^{-1}$. The large surface area of 918 $m^2\ g^{-1}$ (Figure 5c) and pore volume of 0.368 $cm^3\ g^{-1}$ are obtained at the higher temperature of 450 °C with the sufficient decomposition of the anions and the release of as-formed gases. Accordingly, the morphology changes to be compact blocks with observations of smooth surface (Figure 5e) and enhanced XRD peaks (Figure S13). All these results together with other characterizations for PCN-14 strongly confirm the formation of N-enriched ultramicroporous carbon material with large surface area and high N content. Furthermore, a higher carbonization temperature up to 600 °C causes a slight variation of FT-IR and morphology results. The surface area and pore volume gradually decrease with rising temperature (Table S1), accompanied with a certain enhancement of XRD peaks and slight decrease of N content and constant S content (Figure 5d).

The above survey of the carbonization temperature indicates that the large-surface-area ultramicroporous structure with high N content (20.10 wt %) and S content (3.06 wt %) indeed forms at ca. 450 °C. A polytriazine cationic network forms through trimerization at a relatively low temperature, ca. 350 °C. Along with the carbonization process, ultramicropores originate from the decomposition of anions and the release of as-formed gases CF_x and SO_x, which happens in a very sharp temperature range, 440−450 °C (Figure 5c), indicating the key role of the counterion as a "molecular porogen".[45,46] The carbonization of D[4-CNPyMe]Br with Br anion fails to produce any porous structure with the same approach, providing an indirect proof that the [Tf_2N] anion acts as a molecular template.[55] Another precursor D[PyMe]Tf_2N without a cross-linkable cyano group results in a very low yield for

DOI: 10.1021/acsami.5b04842
ACS Appl. Mater. Interfaces 2015, 7, 18508−18518

nonporous carbon, indicating the vital role of CN groups for the described consecutive trimerization and carbonization processes. Furthermore, although presently short of direct evidence, the well-defined crystal structure of the CIS precursor may possibly associate with the formation of the narrow ultramicropores, as suggested by a recently reported crystallized protic salt carbon precursor.[57]

CO_2 Selective Adsorption. Figure 6, parts a and b, show the CO_2 adsorption isotherms of all the synthesized PCN-*xy* series measured at 273 and 298 K, respectively. The corresponding CO_2 adsorption capacities are listed in Table 1. All of these PCN-*xy* carbons show superior CO_2 adsorption capacities (3.59−5.33 mmol g^{-1} at 273 K and 2.35−3.68 mmol g^{-1} at 298 K) at ambient pressure (1.0 bar). The highest CO_2 uptakes, 5.33 mmol g^{-1} (23.5 wt %) at 273 K and 3.68 mmol g^{-1} (16.2 wt %) at 298 K, are achieved on the PCN-14 sample. These data are higher than all the reported CO_2 uptakes over IL-derived porous carbon materials,[47,49,51] and superior or comparable to those over the reported porous materials (typically, N-enriched porous organic polymer,[58] MOP, or MOF-derived porous carbons[15−19,31,59]), but still inferior to those over some carbon adsorbents, including hard-templated carbons[16,37] and physically or chemically activated carbons.[13,14,17,38−40] In particular, at the low pressure 0.15 bar, PCN-14 exhibits very high CO_2 adsorption capacities of 2.58 and 1.50 mmol g^{-1} at 273 and 298 K, respectively. The values are much higher than most of the reported porous carbons for CO_2 capture under identical conditions,[15,18,31,59−61] which is of great significance to broaden its potential application in separating CO_2 from dilute gases.[61] In addition, five-cycling reproducible CO_2 sorption isotherms are observed (Figure S19), suggesting their good regeneration stability for CO_2 capture.

The N_2 adsorption isotherms at 273 K for all the PCN-*xy* samples are measured to investigate their selective adsorption of CO_2 versus N_2, which is crucial for CO_2 capture faced with various practical situations such as mixed gases and dilute CO_2 in the flue gas. CO_2/N_2 selectivities of PCN-*xy* are estimated using initial slope ratios calculated from Henry's law constants for single-component adsorption isotherms at low pressure coverage (Figure S20), which is one of the most common methods to calculate gas selectivities.[32] The corresponding calculation results are described in Figure 6c. All of the samples exhibit very low N_2 uptakes and give high CO_2/N_2 selectivities, which exactly relate to the textural properties and chemical compositions of these carbons. The highest value of 156 is observed over the PCN-14 sample (Figure 6c), mainly due to its high surface area (918 m^2 g^{-1}), narrow ultramicropore (0.59 nm), and high N content (20.10 wt %). Compared with PCN-14, PCN-13 with a similar N content of 20.54 wt % and pore size (0.61 nm) but lower surface area (722 m^2 g^{-1}) gives a lower CO_2/N_2 selectivity of 125. The other carbon samples, including PCN-24, PCN-23, PCN-44, PCN-43, and PCN-64, present much lower CO_2/N_2 selectivities, ranging from 66 to 90, attributable to their lower N contents compared to those of PCN-14 and PCN-13. Although sample PCN-64 has the low N content of 7.04 wt %, it exhibits a considerable CO_2/N_2 selectivity of 74, which may arise from its large surface area and very small pore size of 0.51 nm. In particular, PCN-54 with abundant mesopores only gives a very low CO_2/N_2 selectivity of 29. Low N_2 uptakes are observed over these PCN-*xy* samples even at enhanced pressure (273 K, 1.0 bar). For example, PCN-14 presents an almost negligible N_2 adsorption capacity of ~0.036 mmol g^{-1} (273 K, 1.0 bar). Correspondingly, the CO_2/N_2 adsorption ratio at 1.0 bar is as high as 148 over PCN-14, superior to previous reports (Table S4).[62] The ideal adsorbed solution theory (IAST) method has also been applied to determine the CO_2/N_2 adsorption selectivity of PCN-14 simulated from flue gas mixture (15 wt % CO_2/N_2). The IAST selectivities of CO_2/N_2 of PCN-14 and PCN-13 are estimated to be 142 and 121 at 273 K, 1.0 bar (Figure S21), respectively, which are in reasonable agreement with the values obtained from Henry's constant ratios. Table S4 compares the CO_2/N_2 adsorption selectivities for PCN-14 and PCN-13 with various other porous solid adsorbents. The comparison indicates that the CO_2/N_2 selectivity over PCN-14 is superior to the values of all the reported porous carbons, including templated carbons,[9,10,35,37] chemical activated carbons,[38,40,62] and IL-, MOP- or MOF-derived carbons,[15,16,18,31,47,59] even higher than those of the recently reported highest values over porous organic polymers, e.g., electron-rich oganoniridic framework PECONF-1 (109),[32] azo-covalent organic polymer azo-COP-2 (109.6),[33] benzimidazole-linked porous polymer BILP-2 (113),[63] pyrrole-HCP (117),[64] and Network-7 (119).[65] We note that those MOP materials with high CO_2/N_2 selectivities often exhibited moderate CO_2 uptakes (2−3 mmol g^{-1}, 273 K, 1.0 bar, Table S4). In clear contrast, the current sample PCN-14 simultaneously possesses a high CO_2 uptake of 5.33 mmol g^{-1}, an ultrahigh CO_2/N_2 adsorption ratio (148), and a selectivity (156) at 273 K, which is very impressive in the studies of CO_2 adsorption.

Insight into the Adsorption Behavior. The excellent CO_2 adsorption capacity over the PCN-14 sample can be assigned to the large surface area, high N content, and strictly ultramicroporous structure, which are all beneficial factors, as revealed by previous works.[34−43] The normalized CO_2 uptakes (273 K, 1.0 bar) per unit of surface area or N content are calculated and correlated to the corresponding surface areas and N contents, respectively (Figure S22), and the results show a general, although not exact, trend that the larger surface area and higher N content, the higher CO_2 uptake (The details see the discussion text after Figure S22). Therefore, the PCN-14 sample simultaneously possessing large surface area and high N content presents the highest CO_2 uptake, which is superior to not only the PCN-13 sample with almost the same N content but smaller surface area, but also other PCN-*xy* samples (e.g., PCN-64) with large surface areas but lower N contents. Therefore, the enriched heteroatoms (N, 20.10 wt % and S, 3.06 wt %) codoped in PCN-14 play the key roles in enhancing the high CO_2 adsorption capacity, mainly due to the strong acid−base interaction between acidic CO_2 molecules and basic N sites or S—C functional groups, and the strong pole−pole interactions between the large quadrupole moment of CO_2 molecules and polar sites associated with N- or S-functionalities.[36−39,66] Besides, the CO_2 uptake over PCN-14 with strictly ultramicroporous structure is also higher than those previous hierarchical carbon materials containing both large surface area and high N content.[34,35,47] This observation agrees with the early finding that ultrafinely microporosity with high surface areas and narrow micropores smaller than 0.7 nm can provide more accommodations for trapping CO_2 molecules via a volume-filling mechanism.[40−43,67] Briefly, the strictly ultramicroporous structure of the PCN-14 sample with high surface area and N/S-*co*-doped polar surface deserves the high CO_2 adsorption uptake under ambient pressure.

DOI: 10.1021/acsami.5b04842
ACS Appl. Mater. Interfaces 2015, 7, 18508−18518

The ultrahigh CO_2/N_2 selectivity over PCN-14 can be also assigned to the above-mentioned factors. Generally, gaseous separation selectivity is determined by the thermodynamic and kinetic discrepancy of different gases over the adsorbents. CO_2-philicity is the thermodynamic driving force for the selective adsorption of CO_2 relative to N_2. The high N content over the PCN-14 sample provides strong polar interaction between CO_2 and lone-pair electrons on the N atom, enhancing the CO_2-philicity, which is however neutral toward N_2. This discrepancy ultimately benefits the improvement of CO_2/N_2 selectivity.[33] Similarly, S-doping also promotes the CO_2-philicity but neutrals toward N_2, thus further enhancing the CO_2/N_2 selectivity.[66] However, the ultrahigh CO_2/N_2 selectivity over the PCN-14 sample cannot be merely attributed to the high N-doping content because various other N-enriched carbon materials with large surface areas usually could not offer such a high selectivity (Table S4). In-depth structural analyses indicate that those previous N-enriched carbons all owned certain mesopores, while the PCN-14 sample is of strictly ultramicroporous structure. The narrow ultramicropores centered at 0.59 nm provide sufficiently large differentiation in kinetic diffusion between the small CO_2 molecule (3.30 Å) and the relatively large one of N_2 (3.64 Å), favoring the higher CO_2/N_2 adsorption selectivity.[67] The strictly ultramicroporous structure excludes the possible decline of selectivity ascribed to mesoporosity. The contrastive data over the sample PCN-54 with hierarchical micro/mesoporous structure give another strong support for this speculation: They present the much inferior CO_2/N_2 selectivity of 29 (Figure 6c) compared to those over other PCN-*xy* samples with high ultramicroporosity. In a word, the strictly unique ultramicroporosity plays a critical role for both high adsorption capacity and high selectivity over PCN-*xy* samples.

To further understand the adsorption results, the isosteric heats of adsorption (Q_{st}) are calculated by the Clausius–Clapeyron equation from dual-site Langmuir–Freundlich fits of CO_2 isotherms measured at 273 and 298 K. Figure 5d shows the plot of adsorption enthalpies as a function of the adsorbed CO_2 uptakes. The high Q_{st} values of CO_2 (37–55 kJ mol^{-1}) at low coverage are obtained over these PCN-*xy* samples, surpassing most of the reported values over porous carbons, and comparable to polyamine or imide-functionalized MOPs (e.g., PPN-6-CH_2DETA, TPI-1@IC) (40–63 kJ mol^{-1}).[68,69] With the increase of CO_2 uptake to 0.3 mmol g^{-1}, the isosteric heats present sharp decline, and most of them keep constant at higher CO_2 adsorbed uptakes. The saturated Q_{st} values are retained at a high level (e.g., Q_{st} 49.5 kJ mol^{-1} for PCN-14, Table S5), reflecting the strong CO_2 affinity up to high CO_2 loadings, which is consistent with the large CO_2 adsorption capacities. The highest CO_2 uptake happens over the PCN-14 sample with the highest initial and saturated Q_{st} values. Such high adsorption enthalpies can be attributed to the pyridinic/pyrrolic N and thiophene S enriched polar surface and strictly ultramicropore channels (0.59 nm), indeed reflecting the enhanced quadrupolar interaction between carbon framework and CO_2 molecules, which accounts for the high CO_2 uptake and CO_2/N_2 selectivity.[67,69,70] Besides, the saturated Q_{st} for PCN-14 still locates in the range of strong physisorption or weak chemisorption, causing a good trade-off between adsorption capacity/selectivity and reversibility.[32]

CONCLUSIONS

A new family of molecular level carbon precursors, cyanopyridinium crystalline dicationic salts (CISs), are task-specifically designed and prepared. Through straightforward carbonizing these molecular CISs at the relatively low temperature of 450 °C, series of highly N-enriched ultramicroporous carbons PCN-*xy* with large surface areas are resulted. Neither additives nor pre/post-treatments are required in this process. The porosity and N content of the carbon samples can be precisely tailored by varying the intrinsic chemical structures and compositions of CISs. By virtue of the simultaneous high surface area (918 m^2 g^{-1}), N content (20.10 wt %), and narrow strictly ultramicroporosity (0.59 nm), the lead sample PCN-14 performs exceptionally high CO_2 uptakes at 1.0 bar (5.33 mmol g^{-1} at 273 K and 3.68 mmol g^{-1} at 298 K), superior CO_2/N_2 selectivity (156 at 273 K), and the unprecedented adsorption ratio of CO_2 to N_2 (148 at 273 K and 1 bar). The strict ultramicroporosity and high N-doping content play crucial roles for both high CO_2 adsorption capacity and high selectivity. This straightforward procedure changes the current situation of the inferior CO_2/N_2 selectivity over carbon materials, providing new insights into high-performance porous carbon materials for efficient selective CO_2 capture.

ASSOCIATED CONTENT

Supporting Information

The Supporting Information is available free of charge on the ACS Publications website at DOI: 10.1021/acsami.5b04842.

^{1}H NMR, ^{13}C NMR, XRD, and TGA of CIS precursors. XRD, SEM, and FT-IR of CIS-derived N-doped carbons and their CO_2 adsorption performance (PDF)

AUTHOR INFORMATION

Corresponding Authors

*Tel: +86-25-83172264; fax: +86-25-83172261; e-mail: njutzhouyu@njtech.edu.cn (Y.Z.).

*Tel: +86-25-83172264; fax: +86-25-83172261; e-mail: junwang@njtech.edu.cn (J.W.).

Author Contributions

The manuscript was written through contributions of G.J.C., Y.Z., and J.W. All authors have given approval to the final version of the manuscript.

Notes

The authors declare no competing financial interest.

ACKNOWLEDGMENTS

The authors thank greatly the National Natural Science Foundation of China (Nos. 21136005, 21303084, and 21476109), Jiangsu Provincial Science Foundation for Youths (No. BK20130921), Specialized Research Fund for the Doctoral Program of Higher Education (No. 20133221120002), and the Scientific Research and Innovation Project for College Graduates of Jiangsu Province (CXZZ13_0447).

REFERENCES

(1) Dutta, S.; Bhaumik, A.; Wu, K. C.-W. Hierarchically Porous Carbon Derived from Polymers and Biomass: Effect of Interconnected Pores on Energy Applications. *Energy Environ. Sci.* **2014**, *7*, 3574–3592.

DOI: 10.1021/acsami.5b04842
ACS Appl. Mater. Interfaces 2015, 7, 18508–18518

(2) Wood, K. N.; O'Hayre, R.; Pylypenko, S. Recent Progress on Nitrogen/Carbon Structures Designed for Use in Energy and Sustainability Applications. *Energy Environ. Sci.* **2014**, *7*, 1212−1249.
(3) Parlett, C. M. A.; Wilson, K.; Lee, A. F. Hierarchical Porous Materials: Catalytic Applications. *Chem. Soc. Rev.* **2013**, *42*, 3876−3893.
(4) Wang, J.; Huang, L.; Yang, R.; Zhang, Z.; Wu, J.; Gao, Y.; Wang, Q.; O'Hareb, D.; Zhong, Z. Recent Advances in Solid Sorbents for CO_2 Capture and New Development Trends. *Energy Environ. Sci.* **2014**, *7*, 3478−3515.
(5) Titirici, M.-M.; White, R. J.; Brun, N.; Budarin, V. L.; Su, D. S.; del Monte, F.; Clark, J. H.; MacLachlan, M. J. Sustainable Carbon Materials. *Chem. Soc. Rev.* **2015**, *44*, 250−290.
(6) Ma, T.-Y.; Liu, L.; Yuan, Z.-Y. Direct Synthesis of Ordered Mesoporous Carbons. *Chem. Soc. Rev.* **2013**, *42*, 3977−4003.
(7) Oschatza, L. M.; Kaskel, S. Tailoring Porosity in Carbon Materials for Supercapacitor Applications. *Mater. Horiz.* **2014**, *1*, 157−168.
(8) Wu, D.; Li, Z.; Zhong, M.; Kowalewski, T.; Matyjaszewski, K. Templated Synthesis of Nitrogen-Enriched Nanoporous Carbon Materials from Porogenic Organic Precursors Prepared by ATRP. *Angew. Chem.* **2014**, *126*, 4038−4041.
(9) Li, Z.; Wu, D.; Liang, Y.; Fu, R.; Matyjaszewski, K. Synthesis of Well-Defined Microporous Carbons by Molecular-Scale Templating with Polyhedral Oligomeric Silsesquioxane Moieties. *J. Am. Chem. Soc.* **2014**, *136*, 4805−4808.
(10) Qian, D.; Lei, C.; Wang, E.; Li, W.; Lu, A. A Method for Creating Microporous Carbon Materials with Excellent CO_2-Adsorption Capacity and Selectivity. *ChemSusChem* **2014**, *7*, 291−298.
(11) Gu, Y.; Xiong, Z.; Abdulla, W. A.; Chen, G.; Zhao, X. S. A New Approach to Preparing Porous Carbons with Controllable Pore Structure and Morphology. *Chem. Commun.* **2014**, *50*, 14824−14827.
(12) Fechler, N.; Fellinger, T.-P.; Antonietti, M. Salt Templating": A Simple and Sustainable Pathway Toward Highly Porous Functional Carbons from Ionic Liquids. *Adv. Mater.* **2013**, *25*, 75−79.
(13) Li, Y.; Ben, T.; Zhang, B.; Fu, Y.; Qiu, S. Ultrahigh Gas Storage Both at Low and High Pressures in KOH-Activated Carbonized Porous Aromatic Frameworks. *Sci. Rep.* **2013**, *3*, 2420.
(14) Nandi, M.; Okada, K.; Dutta, A.; Bhaumik, A.; Maruyama, J.; Derks, D.; Uyama, H. Unprecedented CO_2 Uptake over Highly Porous N-doped Activated Carbon Monoliths Prepared by Physical Activation. *Chem. Commun.* **2012**, *48*, 10283−10285.
(15) Zhang, Y.; Li, B.; Williams, K.; Gao, W.; Ma, S. A New Microporous Carbon Material Synthesized via Thermolysis of a Porous Aromatic Framework Embedded with an Extra Carbon Source for Low-Pressure CO_2 Uptake. *Chem. Commun.* **2013**, *49*, 10269−10271.
(16) Li, B.; Zhang, Y.; Ma, D.; Zhu, L.; Zhang, D.; Chrzanowski, M.; Shi, Z.; Ma, S. Creating Extra Pores in Microporous Carbon via a Template Strategy for a Remarkable Enhancement of Ambient-Pressure CO_2 Uptake. *Chem. Commun.* **2015**, *51*, 8683−8686.
(17) Ashourirad, B.; Sekizkardes, A. K.; Altarawneh, S.; El-Kaderi, H. M. Exceptional Gas Adsorption Properties by Nitrogen-Doped Porous Carbons Derived from Benzimidazole-Linked Polymers. *Chem. Mater.* **2015**, *27*, 1349−1358.
(18) Aijaz, A.; Fujiwara, N.; Xu, Q. From Metal-Organic Framework to Nitrogen-Decorated Nanoporous Carbons: High CO_2 Uptake and Efficient Catalytic Oxygen Reduction. *J. Am. Chem. Soc.* **2014**, *136*, 6790−6793.
(19) Srinivas, G.; Krungleviciute, V.; Guo, Z.-X.; Yildirim, T. Exceptional CO_2 Capture in a Hierarchically Porous Carbon with Simultaneous High Surface Area and Pore Volume. *Energy Environ. Sci.* **2014**, *7*, 335−342.
(20) Biswal, M.; Banerjee, A.; Deoab, M.; Ogale, S. From Dead Leaves to High Energy Density Supercapacitors. *Energy Environ. Sci.* **2013**, *6*, 1249−1259.
(21) Zhang, S.; Dokko, K.; Watanabe, M. Carbon Materialization of Ionic Liquids: from Solvents to Materials. *Mater. Horiz.* **2015**, *2*, 168−197.
(22) Yang, H.; Xu, Z.; Fan, M.; Gupta, R.; Slimane, R. B.; Bland, A. E.; Wright, I. Progress in Carbon Dioxide Separation and Capture: A Review. *J. Environ. Sci.* **2008**, *20*, 14−27.
(23) Rochelle, G. T. Amine Scrubbing for CO_2 Capture. *Science* **2009**, *325*, 1652−1654.
(24) D'Alessandro, D. M.; Smit, B.; Long, J. R. Carbon Dioxide Capture: Prospects for New Materials. *Angew. Chem., Int. Ed.* **2010**, *49*, 6058−6082.
(25) Choi, S.; Drese, J. H.; Jones, C. W. Adsorbent Materials for Carbon Dioxide Capture from Large Anthropogenic Point Sources. *ChemSusChem* **2009**, *2*, 796−854.
(26) Xu, X.; Song, C.; Andresen, J. M.; Miller, B. G.; Scaroni, A. W. Novel Polyethylenimine-Modified Mesoporous Molecular Sieve of MCM-41 Type as High-Capacity Adsorbent for CO_2 Capture. *Energy Fuels* **2002**, *16*, 1463−1469.
(27) Zhang, Z.; Yao, Z.; Xiang, S.; Chen, B. Perspective of Microporous Metal-Organic Frameworks for CO_2 Capture and Separation. *Energy Environ. Sci.* **2014**, *7*, 2868−2899.
(28) Dawson, R.; Stöckel, E.; Holst, J. R.; Adams, D. J.; Cooper, A. I. Microporous Organic Polymers for Carbon Dioxide Capture. *Energy Environ. Sci.* **2011**, *4*, 4239−4245.
(29) Lu, A.; Hao, G. Porous Materials for Carbon Dioxide Capture. *Annu. Rep. Prog. Chem., Sect. A: Inorg. Chem.* **2013**, *109*, 484−503.
(30) Komatsu, S. T.; Fujita, S. J. High-Pressure Adsorption Equilibria of Methane and Carbon Dioxide on Several Activated Carbons. *J. Chem. Eng. Data* **2005**, *50*, 369−376.
(31) Gadipelli, S.; Guo, Z. X. Tuning of ZIF-Derived Carbon with High Activity, Nitrogen Functionality, and Yield-a Case for Superior CO_2 Capture. *ChemSusChem* **2015**, *8*, 2123−2132.
(32) Mohanty, P.; Kull, L. D.; Landskron, K. Porous Covalent Electron-Rich Organonitridic Frameworks as Highly Selective Sorbents for Methane and Carbon Dioxide. *Nat. Commun.* **2011**, *2*, 401.
(33) Patel, H. A.; Je, S. H.; Park, J.; Chen, D. P.; Jung, Y.; Yavuz, C. T.; Coskun, A. Unprecedented High-Temperature CO_2 Selectivity in N_2-Phobic Nanoporous Covalent Organic Polymers. *Nat. Commun.* **2013**, *4*, 1357.
(34) Li, Q.; Yang, J.; Feng, D.; Wu, Z.; Wu, Q.; Park, S. S.; Ha, C.-S.; Zhao, D. Facile Synthesis of Porous Carbon Nitride Spheres with Hierarchical Three-Dimensional Mesostructures for CO_2 Capture. *Nano Res.* **2010**, *3*, 632−642.
(35) Wei, J.; Zhou, D.; Sun, Z.; Deng, Y.; Xia, Y.; Zhao, D. A Controllable Synthesis of Rich Nitrogen-Doped Ordered Mesoporous Carbon for CO_2 Capture and Supercapacitors. *Adv. Funct. Mater.* **2013**, *23*, 2322−2328.
(36) Hao, G.; Li, W.; Qian, D.; Lu, A. Rapid Synthesis of Nitrogen-Doped Porous Carbon Monolith for CO_2 Capture. *Adv. Mater.* **2010**, *22*, 853−857.
(37) Xia, Y.; Mokaya, R.; Walker, G. S.; Zhu, Y. Superior CO_2 Adsorption Capacity on N-Doped, High-Surface-Area, Microporous Carbons Template from Zeolite. *Adv. Energy Mater.* **2011**, *1*, 678−683.
(38) Sevilla, M.; Valle-Vigón, P.; Fuertes, A. B. N-doped Polypyrrole-Based Porous Carbons for CO_2 Capture. *Adv. Funct. Mater.* **2011**, *21*, 2781−2787.
(39) Xing, W.; Liu, C.; Zhou, Z.; Zhang, L.; Zhou, J.; Zhuo, S.; Yan, Z.; Gao, H.; Wang, G.; Qiao, S. Superior CO_2 Uptake of N-Doped Activated Carbon through Hydrogen-Bonding Interaction. *Energy Environ. Sci.* **2012**, *5*, 7323−7327.
(40) Sevilla, M.; Fuertes, A. B. Sustainable Porous Carbons with a Superior Performance for CO_2 Capture. *Energy Environ. Sci.* **2011**, *4*, 1765−1771.
(41) Wickramaratne, N. P.; Jaroniec, M. Importance of Small Micropores in CO_2 Capture by Phenolic Resin-Based Activated Carbon Spheres. *J. Mater. Chem. A* **2013**, *1*, 112−116.
(42) Sevilla, M.; Parra, J. B.; Fuertes, A. B. Assessment of the Role of Micropore Size and N-Doping in CO_2 Capture by Porous Carbons. *ACS Appl. Mater. Interfaces* **2013**, *5*, 6360−6368.

DOI: 10.1021/acsami.5b04842
ACS Appl. Mater. Interfaces 2015, 7, 18508−18518

(43) Zhang, Z.; Zhou, J.; Xing, W.; Xue, Q.; Yan, Z.; Zhuo, S.; Qiao, S. Critical Role of Small Micropores in High CO_2 Uptake. *Phys. Chem. Chem. Phys.* **2013**, *15*, 2523−2529.
(44) Rondeau-Gagné, S.; Morin, J.-F. Preparation of Carbon Nanomaterials from Molecular Precursors. *Chem. Soc. Rev.* **2014**, *43*, 85−98.
(45) Lee, J. S.; Wang, X.; Luo, H.; Baker, G. A.; Dai, S. Facile Ionothermal Synthesis of Microporous and Mesoporous Carbons from Task Specific Ionic Liquids. *J. Am. Chem. Soc.* **2009**, *131*, 4596−4597.
(46) Fulvio, P. F.; Hillesheim, P. C.; Oyola, Y.; Mahurin, S. M.; Veithb, G. M.; Dai, S. *Chem. Commun.* **2013**, *49*, 7289−7291.
(47) Mahurin, S. M.; Fulvio; Hillesheim, P. F.; P, C.; Nelson, K. M.; Veith, G. M.; Dai, S. Directed Synthesis of Nanoporous Carbons from Task-Specific Ionic Liquid Precursors for the Adsorption of CO_2. *ChemSusChem* **2014**, *7*, 3284−3289.
(48) Zhang, S.; Miran, M. S.; Ikoma, A.; Dokko, K.; Watanabe, M. Protic Ionic Liquids and Salts as Versatile Carbon Precursors. *J. Am. Chem. Soc.* **2014**, *136*, 1690−1693.
(49) Zhang, S.; Dokko, K.; Watanabe, M. Direct Synthesis of Nitrogen-Doped Carbon Materials from Protic Ionic Liquids and Protic Salts: Structural and Physicochemical Correlations between Precursor and Carbon. *Chem. Mater.* **2014**, *26*, 2915−2926.
(50) Paraknowitsch, J. P.; Zhang, J.; Su, D.; Thomas, A.; Antonietti, M. Ionic Liquids as Precursors for Nitrogen-Doped Graphitic Carbon. *Adv. Mater.* **2010**, *22*, 87−92.
(51) Zhu, X.; Hillesheim, P. C.; Mahurin, S. M.; Wang, C.; Tian, C.; Brown, S.; Luo, H.; Veith, G. M.; Han, K. S.; Hagaman, E. W.; Liu, H.; Dai, S. Efficient CO_2 Capture by Porous, Nitrogen-Doped Carbonaceous Adsorbents Derived from Task-Specific Ionic Liquids. *ChemSusChem* **2012**, *5*, 1912−1917.
(52) Paraknowitsch, J. P.; Thomas, A.; Antonietti, M. A Detailed View on the Polycondensation of Ionic Liquid Monomers towards Nitrogen Doped Carbon Materials. *J. Mater. Chem.* **2010**, *20*, 6746−6758.
(53) Zhang, P.; Sun, F.; Xiang, Z.; Shen, Z.; Yun, J.; Cao, D. ZIF-Derived in situ Nitrogen-Doped Porous Carbons as Efficient Metal-Free Electrocatalysts for Oxygen Reduction Reaction. *Energy Environ. Sci.* **2014**, *7*, 442−450.
(54) Kuhn, P.; Antonietti, M.; Thomas, A. Porous, Covalent Triazine-Based Frameworks Prepared by Ionothermal Synthesis. *Angew. Chem., Int. Ed.* **2008**, *47*, 3450−3453.
(55) Zhao, Q.; Fellinger, T.; Antonietti, M.; Yuan, J. A Novel Polymeric Precursor for Micro/Mesoporous Nitrogen-Doped Carbons. *J. Mater. Chem. A* **2013**, *1*, 5113−5120.
(56) Hu, X.; Chen, Q.; Zhao, Y.; Laursenb, B. W.; Han, B. Straightforward Synthesis of a Triazine-Based Porous Carbon with High Gas-Uptake Capacities. *J. Mater. Chem. A* **2014**, *2*, 14201−14208.
(57) Zhang, S.; Mandai, T.; Ueno, K.; Dokko, K.; Watanabe, M. Hydrogen-Bonding Supramolecular Protic Salt as an "All-In-One" Precursor for Nitrogen-Doped Mesoporous Carbons for CO_2 Adsorption. *Nano Energy* **2015**, *13*, 376−386.
(58) Zhu, X.; Mahurin, S. M.; An, S.; Do-Thanh, C.-L.; Tian, C.; Li, Y.; Gill, L. W.; Hagaman, E. W.; Bian, Z.; Zhou, J.; Hu, J.; Liu, H.; Dai, S. Efficient CO_2 Capture by a Task-Specific Porous Organic Polymer Bifunctionalized with Carbazole and Triazine Groups. *Chem. Commun.* **2014**, *50*, 7933−7936.
(59) Aijaz, A.; Akita, T.; Yang, H.; Xu, Q. From Ionic-Liquid@Metal-Organic Framework Composites to Heteroatom-Decorated Large-Surface Area Carbons: Superior CO_2 and H_2 Uptake. *Chem. Commun.* **2014**, *50*, 6498−6501.
(60) Hao, G.; Li, W.; Qian, D.; Wang, G.; Zhang, W.; Zhang, T.; Wang, A.; Schüth, F.; Bongard, H.; Lu, A. Structurally Designed Synthesis of Mechanically Stable Poly (benzoxazine-co-resol)-Based Porous Carbon Monoliths and Their Application as High-Performance CO_2 Capture Sorbents. *J. Am. Chem. Soc.* **2011**, *133*, 11378−11388.
(61) Hao, G.; Jin, Z.; Sun, Q.; Zhang, X.; Zhang, J.; Lu, A. Porous Carbon Nanosheets with Precisely Tunable Thickness and Selective CO_2 Adsorption Properties. *Energy Environ. Sci.* **2013**, *6*, 3740−3747.
(62) Wang, J.; Liu, Q. An Efficient One-Step Condensation and Activation Strategy to Synthesize Porous Carbons with Optimal Micropore Sizes for Highly Selective CO_2 Adsorption. *Nanoscale* **2014**, *6*, 4148−4156.
(63) Rabbani, M. G.; El-Kaderi, H. M. Synthesis and Characterization of Porous Benzimidazole-Linked Polymers and Their Performance in Small Gas Storage and Selective Uptake. *Chem. Mater.* **2012**, *24*, 1511−1517.
(64) Luo, Y.; Li, B.; Wang, W.; Wu, K.; Tan, B. Hypercrosslinked Aromatic Heterocyclic Microporous Polymers: a New Class of Highly Selective CO_2 Capturing Materials. *Adv. Mater.* **2012**, *24*, 5703−5707.
(65) Yao, S.; Yang, X.; Yu, M.; Zhang, Y.; Jiang, J. High Surface Area Hypercrosslinked Microporous Organic Polymer Networks Based on Tetraphenylethylene for CO_2 Capture. *J. Mater. Chem. A* **2014**, *2*, 8054−8059.
(66) Kiciński, W.; Szalaa, M.; Bystrzejewski, M. Sulfur-Doped Porous Carbons: Synthesis and Applications. *Carbon* **2014**, *68*, 1−32.
(67) Zhou, J.; Li, Z.; Xing, W.; Zhu, T.; Shen, H.; Zhuo, S. N-doped Microporous Carbons Derived from Direct Carbonization of K^+ Exchanged Meta-Aminophenol-Formaldehyde Resin for Superior CO_2 Sorption. *Chem. Commun.* **2015**, *51*, 4591−4594.
(68) Lu, W.; Sculley, J. P.; Yuan, D.; Krishna, R.; Wei, Z.; Zhou, H. Polyamine-Tethered Porous Polymer Networks for Carbon Dioxide Capture from Flue Gas. *Angew. Chem., Int. Ed.* **2012**, *51*, 7480−7484.
(69) Wu, S.; Gu, S.; Zhang, A.; Yu, G.; Wang, Z.; Jian, J.; Pan, C. A Rational Construction of Microporous Imide-Bridged Covalent-Organic Polytriazines for High-Enthalpy Small Gas Absorption. *J. Mater. Chem. A* **2015**, *3*, 878−885.
(70) Germain, J.; Fréchet, J. M. J.; Svec, F. Nanoporous Polymers for Hydrogen Storage. *Small* **2009**, *5*, 1098−1111.

DOI: 10.1021/acsami.5b04842
ACS Appl. Mater. Interfaces 2015, 7, 18508−18518